Inorganic Chemistry

Article

pubs.acs.org/IC

Tuning the Emission Lifetime in Bis-cyclometalated Iridium(III) Complexes Bearing Iminopyrene Ligands

Ashlee J. Howarth,[†] David L. Davies,[‡] Francesco Lelj,[§] Michael O. Wolf,*[,†] and Brian O. Patrick[†]

[†]Department of Chemistry, University of British Columbia, Vancouver, British Columbia V6T 1Z1, Canada

[‡]Department of Chemistry, University of Leicester, University Road, Leicester LE1 7RH, U.K.

[§]La.M.I. and LaSCAMM, INSTM Sezione Basilicata, Dipartimento di Scienze, Università della Basilicata, Via dell'Ateneo Lucano 10, 85100 Potenza, Italy

Supporting Information

ABSTRACT: Bis-cyclometalated Ir(III) complexes with the general formula $Ir(ppz)_2(X^NPyrene)$, where ppz = 1-phenylpyrazole and X^NPyrene is a bidentate chelate with X = N or O, are reported. Modifications on the ancillary ligand containing pyrene drastically affect the emission lifetimes observed (0.329 to 104 μs). Extended emission lifetimes in these complexes compared to model complexes result from reversible electronic energy transfer or the observation of dual emission containing along-lived pyrene ligand-centered triplet (^{3}LC) component. A combination of steady-state and time-resolved spectroscopic techniques are used to observe reversible electronic energy transfer in solution between the iridium core and pyrene moiety in the complex $[Ir(ppz)_2(N_{Me}^NCH_2Pyr)][PF_6]$ (**2**), where $N_{Me}^NCH_2Pyr$ = *N*-(pyren-1-ylmethyl)-1-(pyridin-2-yl)ethaneimine. Studies on $[Ir(ppz)_2(N_{Me}^NCH_2Pyr)][PF_6]$ in a poly(methyl methacrylate) (PMMA) film reveal that reversible energy transfer is no longer effective, and instead, dual emission with a long-lived ^{3}LC component from pyrene is observed. Dual emission is observed in additional cyclometalated iridium complexes bearing pyrene-containing ancillary ligands N^NPyrene and O^NPyrene when the complexes are dispersed in a PMMA film.

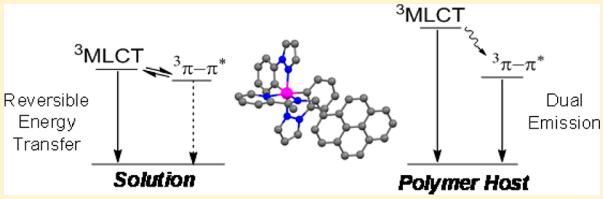

INTRODUCTION

Coordination complexes with long-lived excited states are of interest for applications in lifetime-based imaging to increase signal-to-noise ratios,[1] and in photoredox catalysis[2] and upconversion to enable efficient diffusion-based quenching of a sensitizer.[3] These applications are all currently limited by the lack of materials with appropriate emission or excited state lifetimes. For example, coordination complexes embedded in polymer nanoparticles have been used in time-resolved luminescence bioimaging techniques;[4] however, the dynamic range is currently limited by the lifetime of the phosphors, and species with longer lifetimes in the microsecond or millisecond time regime that emit in a solid-state polymer environment are being sought. In general, organic chromophores show very long phosphorescence lifetimes but are very poorly emissive due to the spin-forbidden nature of the triplet-singlet transition.[5] In contrast, coordination complexes with strong spin−orbit coupling often exhibit reasonably intense phosphorescence (triplet metal-to-ligand charge transfer, ^{3}MLCT, or triplet ligand-to-ligand charge transfer, ^{3}LLCT), but the emission lifetimes are typically short (<1 μs). To overcome these inherent limitations, two approaches can be considered for the design of long lifetime phosphorescent dyes. One approach involves using a ligand-based triplet energy reservoir to extend the lifetime of an emissive ^{3}MLCT state. This tactic has been demonstrated in ruthenium polypyridyl complexes in solution[6] but has rarely been reported for iridium complexes,[7] and it has not been established whether this approach is viable in a polymer matrix. A second approach involves taking advantage of spin−orbit coupling to increase the quantum yield of formally spin-forbidden phosphorescence from an organic emitter. Using this approach, long-lived pyrene phosphorescence has been observed in the solid state by the addition of a mercury trifunctional Lewis acid to pyrene, creating a sandwich complex,[8] as well as in coordination complexes in solution where the organic emitter is directly coordinated to the metal.[9] In rare cases, dual emission is observed from both ^{3}MLCT and ^{3}LC states. In these cases, emission decay is biexponential with a short (^{3}MLCT) and long-lived (^{3}LC) component present.[10]

For bioimaging applications, an important goal is to obtain coordination complexes with long emission lifetimes. In these applications, coordination complexes are often delivered to target tissues encapsulated in a polymeric vessel to help minimize toxicity as well as increase cellular uptake and provide target specificity.[4b] We designed cyclometalated iridium complexes **1**−**3** containing pyrene based ancillary ligands, $Ir(ppz)_2(X^NPyrene)$ (X = N or O) to probe how changes in ancillary ligand structure can alter the photophysical properties. Cyclometalated iridium complexes can demonstrate a range of emissive states including MLCT, ILCT, and LLCT states,[11] allowing the emission energy to be easily tuned. Pyrene is a

Received: May 2, 2014
Published: October 27, 2014

   dx.doi.org/10.1021/ic501032t | *Inorg. Chem.* 2014, 53, 11882−11889

well-studied polyaromatic hydrocarbon; however, the lowest energy singlet state (S_1) is the focus of most applications, while phosphorescence from the lowest-energy triplet state (T_1) has rarely been harnessed.[12] Three main scenarios are possible in coordination complexes bearing pyrene-containing ligands: (a) the ^{3}MLCT state lies lower in energy than the ^{3}pyrene state and ^{3}MLCT emission is observed, (b) the ^{3}MLCT and ^{3}pyrene states are close in energy allowing thermal equilibration between the states such that long-lived ^{3}MLCT emission is observed[6] or (c) the ^{3}pyrene state lies lower than the ^{3}MLCT state and with sufficient spin−orbit coupling long-lived ^{3}pyrene emission can be observed (Scheme 1). In rare cases, dual emission from both ^{3}MLCT and ^{3}pyrene states may be observed.[10] Complexes in categories (b) or (c) are expected to have extended emission lifetimes compared to those in category (a), as a result of contributions to the excited state lifetime from the long-lived ^{3}pyrene chromophore. Herein, we report iridium complexes with extended emission lifetimes in poly(methyl methacrylate) (PMMA) films, resulting from spin−orbit coupling effects and molecular rigidity, which allow for the observation of very long-lived pyrene-based (^{3}LC) phosphorescence (scenario c). In solution, one of the complexes studied shows an extended emission lifetime as a result of the "triplet reservoir effect" (scenario b).

Scheme 1. Three Scenarios for Relative ^{3}MLCT and ^{3}Pyrene ($\pi-\pi^*$) Energy Levels[a]

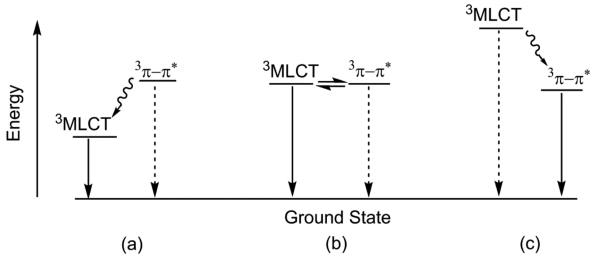

[a]Dashed arrows represent non-radiative decay and solid arrows represent radiative decay pathways.

EXPERIMENTAL SECTION

All experiments were performed under an inert nitrogen atmosphere, using standard Schlenk-line techniques. Deuterated solvents were purchased from Cambridge Isotope Laboratories Inc. Chloro(1-phenylpyrazole)iridium(III) dimer $[IrCl(ppz)_2]_2$,[13] 1-nitropyrene,[14] 1-aminopyrene[15] 2-((pyren-1-ylimino)methyl)phenol (O^NPyr),[16] $[Ir(ppz)_2(N_{Me}\text{^}NPyr)][PF_6]$ (**1**)[17] where N_{Me}^NPyr = *N*-(pyren-1-yl)-1-(pyridin-2-yl)ethaneimine and $[Ir(ppz)_2(N\text{^}NiPr)][PF_6]$ (**5**)[18] where N^NiPr = *N*-isopropyl-1-(pyridin-2-yl)ethaneimine were prepared according to literature procedures. All other solvents and reagents were obtained from commercial sources and used as received. ^{1}H NMR and ^{13}C NMR spectra were obtained using a Bruker AV-400 spectrometer and referenced to the residual protonated solvent peak. High-resolution (HR) electrospray ionization (ESI) mass spectra (MS) were obtained on a Bruker Esquire LC ion trap mass spectrometer. Microwave reactions were performed on a Biotage Initiator 2.5 microwave synthesizer. Film thickness was measured using a Mitutoyo SurfTest SJ-500 profilometer. Absorption spectra were obtained on a Varian Cary 5000 UV−vis-near-IR spectrophotometer. Fluorescence spectra were collected on a Photon Technology International QuantaMaster fluorimeter. Transient absorption spectra were collected using a Princeton Instruments Spectra Pro 2300i Imaging Triple Grating Monochromator/Spectrograph with a Hamamatsu Dynamic Range Streak Camera (excitation source: EKSPLA Nd:YAG laser, λ_{ex} = 355 nm, (full width at half-maximum = 35 ps). Absolute quantum yields were determined using an integrating sphere coupled to the PTI fluorimeter. PMMA films were drop cast from dichloromethane.

X-ray crystallographic analyses were performed by Dr. B. Patrick on a Bruker APEX DUO diffractometer with graphite monochromated Mo Kα radiation. The data were collected to a maximum 2θ value of 55.9° and 53.0° in a series of ϕ and ω scans in 0.5° oscillations using 10.0 s and 30.0 s exposures for **2** and **3**, respectively. Data were collected and integrated using the Bruker SAINT[19] software packages. Data were corrected for Lorentz and polarization effects. **2** crystallizes as a two-component "split-crystal" with components one and two related by a 2.4° rotation about the real axis. Data were integrated for both twin components, including both overlapped and nonoverlapped reflections. In total 63 183 reflections were integrated (26 346 from component one only, 26 083 from component two only, 10 754 overlapped). The linear absorption coefficient, μ, for Mo Kα radiation is 36.32 cm^{-1}. Data were corrected for absorption effects using the multiscan technique (TWINABS[20]), with minimum and maximum transmission coefficients of 0.673 and 0.930, respectively. For complex **3**, of the 33 283 reflections that were collected, 12 990 were unique (R_{int} = 0.054); equivalent reflections were merged. The linear absorption coefficient, μ, for Mo Kα radiation is 42.81 cm^{-1}. Data were corrected for absorption effects using the multiscan technique (SADABS[21]), with minimum and maximum transmission coefficients of 0.693 and 0.918, respectively.

Density functional theory (DFT) calculations were performed using the hybrid xc functional B3LYP.[22] As this functional has been shown to have some drawbacks because of the wrong asymptotic behavior; the 1 parameter xc functionals mPW1PW91[23] and PB1PBE[24] and the asymptotic corrected hybrid functional CAM-B3LYP[25] as well as the meta-hybrid M06, M02X[26] were also applied. For all second period atoms the Dunning[27] all electron basis set augmented by a set of d polarization functions (D95(d)) were used. Hydrogen atoms not involved in any hydrogen bond were described by the same Dunning basis set that does not include p polarization functions. For Ir the new double ζ Stuttgart[28] basis set including f polarization functions and relativistic effects by a fully relativistic small core pseudopotential[24] (SDD09) were used and not the default SDD as included in Gaussian09. The ultrafine option with 99590 grid points was used for the integral calculations for all atoms except Ir where a total of 1 566 228 grid points were used. The first triplet state geometries were computed at the unrestricted level. Singlet and triplet excitations were computed with the time-dependent (TD) DFT linear response approach in the Random Phase Approximation.[29] Analysis of the multideterminental wave functions involved in the transitions was performed using the natural transition orbital approach.[30] All calculations were performed using Gaussian09,[31] version C01 and D01.

Synthesis of $[Ir(ppz)_2(N_{Me}\text{^}NCH_2Pyr)][PF_6]$ (2). $[IrCl(ppz)_2]_2$ (0.070 g, 0.068 mmol), 2-acetylpyridine (0.017 mL, 0.15 mmol), 1-pyrenemethylamine hydrochloride (0.0402 g, 0.150 mmol) and potassium hexafluorophosphate (0.025 g, 0.14 mmol) were placed in a microwave vial with 3.5 mL of ethanol. The suspension was degassed with nitrogen for 4 min. The vial was placed in the microwave reactor and heated under microwave irradiation for 30 min at 100 °C (18 bar, 155 W). The solvent was then removed *in vacuo*, and the solid residue dissolved in 10 mL of CH_2Cl_2. The resulting deep red solution was passed through a Celite pad, and the filtrate was reduced in volume. Layering with hexanes yielded the desired product as a red powder. The product was purified by column chromatography using first MeCN to elute any unreacted 1-pyrenemethylamine and then MeCN/H_2O/$KNO_{3(aq)}$ (96:3:1) to elute the complex as a nitrate salt. Salt metathesis with KPF_6 was performed to obtain complex **2** (0.030 g, yield 46%). ^{1}H NMR (CD_3CN, 400 MHz, proton numbering is the same as in the X-ray structure): δ 8.41 (1H, d, J = 8.3, H_4), 8.36 (1H, d, J = 3.1, H_{26}), 8.38−7.94 (9H, m, $H_{3,29,1,11,23,24,20,21,22}$), 7.84 (1H, d, J = 2.2, H_{25}), 7.76 (1H, d, J = 9.4, H_{10}), 7.63 (1H, t, J = 7.7, H_2), 7.55 (1H, d, J = 8.1, H_{16}), 7.47 (1H, d, J = 2.9, H_{34}), 7.40−7.38 (1H, m, H_{38}), 7.01 (1H, d, J = 2.4, H_{36}), 6.99−6.95 (1H, m, H_{39}), 6.77−6.73

dx.doi.org/10.1021/ic501032t | Inorg. Chem. 2014, 53, 11882−11889

Chart 1. Complexes 1−5

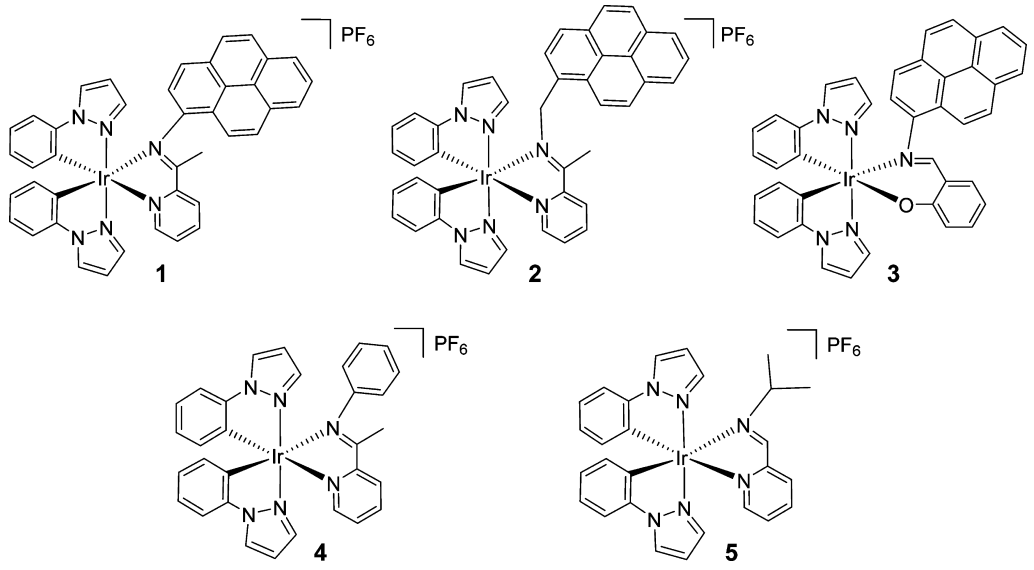

(2H, m, $H_{40,27}$), 6.61 (1H, d, J = 7.9, H_{15}), 6.58 (1H, t, J = 2.2, H_{35}), 6.36−6.32 (1H, m, H_{31}), 6.13−6.11 (3H, m, $H_{8a,8b,30}$), 6.00 (1H, dd, J = 7.6, 1.2, H_{41}), 5.69 (1H, d, J = 4.0, H_{32}), 2.90 (3H, s, H_{7abc}). ^{13}C NMR (CD_3CN, 100 MHz): 139.83−124.16 (overlap $C_{3,29,1,11,23,24,20,21,22}$), 139.0 ($C_{25}$), 138.6 ($C_{36}$), 132.9 ($C_{41}$), 132.6 ($C_{30}$), 129.4 ($C_2$), 128.6 ($C_4$), 127.8 ($C_{26}$), 126.9 ($C_{34}$), 126.6 ($C_{27}$), 126.5 ($C_{31}$), 123.8 ($C_{39}$), 123.4 ($C_{16}$), 122.6 ($C_{10}$), 121.4 ($C_{15}$), 111.3 ($C_{38}$), 110.1 ($C_{32}$), 108.5 ($C_{35}$), 108.1 ($C_{40}$), 57.1 ($C_{8a/b}$), 16.1 ($C_7$). HR ESI-MS: Calcd for $C_{42}H_{32}N_6Ir$: 811.2294; Found: 811.2289 $[M]^+$.

Synthesis of Ir(ppz)$_2$(O^NPyr) (3). $[IrCl(ppz)_2]_2$ (0.070 g, 0.068 mmol), O^NPyr (0.048, 0.15 mmol) and sodium carbonate (0.016 g, 0.15 mmol) were placed in a microwave vial with 3.5 mL of ethanol. The suspension was degassed with nitrogen for 4 min. The vial was placed in the microwave reactor and heated under microwave irradiation for 30 min at 100 °C (18 bar, 155 W). The solvent was then removed *in vacuo*, and the solid residue was dissolved in 10 mL of CH_2Cl_2. The resulting dark yellow solution was passed through a Celite pad, and the filtrate was reduced to approximately 2 mL in volume. Layering with hexanes yielded the desired product as a dark yellow precipitate. The product was purified by column chromatography using first CH_2Cl_2 to elute any unreacted O^NPyr and then EtOAc/CH_2Cl_2 (2:1) to elute complex **3** (0.027 g, yield 50%). ^{1}H NMR (CD_2Cl_2, 400 MHz, proton numbering is the same as in the X-ray structure): δ 8.30 (1H, s, H_7), 8.17 (1H, d, J = 2.6, H_{26}), 8.13−8.11 (2H, m, $H_{21,24}$), 8.06 (1H, d, J = 7.3, H_{22}), 7.98−7.92 (3H, m, $H_{15,23,35}$), 7.86 (1H, d, J = 8.7, H_{14}), 7.76 (1H, d, J = 8.1, H_{19}), 7.59 (1H, d, J = 9.3, H_{10}), 7.52 (1H, d, J = 8.1, H_{20}), 7.36−7.33 (2H, m, $H_{2,33}$), 7.25 (1H, d, J = 8.1, H_{37}), 7.16 (1H, d, J = 7.8, H_4), 7.03 (1H, d, J = 9.3, H_9), 6.88 (1H, t, J = 7.7, 7.5, H_{38}), 6.77−6.74 (2H, m, $H_{1,25}$), 6.68−6.65 (2H, m, $H_{34,39}$), 6.43 (1H, t, J = 7.3, 7.3, H_3), 6.19−6.14 (2H, m, $H_{28,40}$), 6.03−5.99 (2H, m, $H_{29,30}$), 5.90 (1H, d, J = 8.3 H_{31}). ^{13}C NMR (CD_2Cl_2, 100 MHz): 139.5 (C_{24}), 137.9 (C_{35}), 136.4 (C_4), 135.7 (C_{30}), 135.1 (C_2), 134.4 (C_{40}), 127.5 (C_{14}), 127.3 (C_{15}), 127.1 (C_{10}), 127.0 (C_{26}), 126.9 (C_{23}), 125.9 (C_{33}), 125.8 (C_{34}), 125.0 (C_{21}), 124.9 (C_{28}), 124.7 (C_{22}), 124.5 (C_{25}), 123.9 (C_{19}), 122.2 (C_{20}), 122.1 (C_{38}), 121.3 (C_9), 120.4 (C_{29}), 113.9 (C_3), 111.3 (C_{37}), 109.4 (C_{31}), 107.6 (C_1), 107.3 (C_{39}). HR ESI-MS: Calcd for $C_{41}H_{29}N_5OIr$: 798.1978; Found: 798.1966 $[M + H]^+$.

Synthesis of [Ir(ppz)$_2$(N$_{Me}$^NPh)][PF$_6$] (4) where N$_{Me}$^NPh = *N*-phenyl-1-(pyridin-2-yl)ethaneimine. $[IrCl(ppz)_2]_2$ (0.070 g, 0.068 mmol), 2-acetylpyridine (0.017 mL, 0.15 mmol), aniline (0.014 mL, 0.150 mmol), and potassium hexafluorophosphate (0.025 g, 0.14 mmol) were placed in a microwave vial with 3.5 mL of ethanol. The suspension was degassed with nitrogen for 4 min. The vial was placed in the microwave reactor and heated under microwave irradiation for 30 min at 100 °C (18 bar, 155 W). The solvent was then removed *in vacuo*, and the solid residue was dissolved in 10 mL of CH_2Cl_2. The resulting orange solution was passed through a Celite pad, and the filtrate was reduced in volume. Layering with hexanes yielded the desired product as an orange powder. The product was purified by column chromatography using MeCN to elute any unreacted aniline and then MeCN/H_2O/$KNO_{3(aq)}$ (96:3:1) to elute the complex as a nitrate salt. Salt metathesis with KPF_6 was performed to obtain complex **4** (0.053 g, yield 48%). ^{1}H NMR (CD_3CN, 400 MHz, proton numbering is shown in Supporting Information, Figure S1): δ 8.41 (1H, d, J = 2.7, H_{25}), 8.34 (1H, d, J = 8.0, H_4), 8.27 (1H, d, J = 2.7, H_{16}), 8.21−8.12 (3H, m, $H_{1,3,23}$), 7.77 (1H, d, J = 2.2, H_{14}), 7.59 (1H, t, J = 6.7, H_2), 7.44 (1H, d, J = 7.8, H_{18}), 7.36 (1H, d, J = 8.0, H_{27}), 7.09−7.03 (2H, m, $H_{11,19}$), 7.01−6.90 (2H, m, $H_{12,28}$), 6.90−6.79 (2H, m, $H_{20,24}$), 6.76−6.65 (3H, m, $H_{13,15,29}$), 6.46 (1H, t, J = 5.3, H_{10}), 6.25 (1H, dd, J = 7.4, 1.2, H_{21}), 6.02 (1H, dd, J = 7.6, 1.2, H_{30}), 5.84 (1H, dd, J = 7.4, 1.0, H_9), 2.57 (3H, s, H_{7abc}). ^{13}C NMR (CD_3CN, 100 MHz): 151.6 ($C_{1\text{ or }3\text{ or }23}$), 147.5 ($C_{18}$), 140.4 ($C_{1\text{ or }3\text{ or }23}$), 139.5 ($C_{14}$), 138.3 ($C_{1\text{ or }3\text{ or }23}$), 132.9 ($C_{21}$), 132.4 ($C_{30}$), 131.6 ($C_9$), 129.6 ($C_2$), 129.1 ($C_4$), 128.7 ($C_{11\text{ or }19}$), 127.5 (overlap $C_{16\text{ and }25}$), 126.6 ($C_{20\text{ or }24}$), 126.2 ($C_{11\text{ or }19}$), 125.8 ($C_{20\text{ or }24}$), 125.4 ($C_{13\text{ or }15\text{ or }29}$), 124.6 ($C_{10}$), 122.9 ($C_{12\text{ or }28}$), 122.1 ($C_{13\text{ or }15\text{ or }29}$), 111.2 ($C_{27}$), 107.9 ($C_{13\text{ or }15\text{ or }29}$), 18.4 ($C_7$). HR ESI-MS: Calcd for $C_{31}H_{26}N_6Ir$: 673.1825; Found: 673.1827 $[M]^+$.

RESULTS AND DISCUSSION

Complexes **1**−**3** were synthesized according to previously reported methods[17,32] by reacting $[IrCl(ppz)_2]_2$ and the corresponding ligand or ligand precursors under microwave irradiation for 30 min at 100 °C. For comparison with **1**−**3**, model complex **4** was synthesized in an analogous fashion to that of **5**, as previously reported.[18] The syntheses were carried out under microwave irradiation[13,33] giving high yields in short times. The complexes were then purified by column chromatography eluting with an aqueous KNO_3 solution in MeCN and then converted by metathesis back to PF_6 salts. Complexes **1**[17] and **5**[18] have been characterized previously, and atropisomer "a"[17] of complex **1** was used in the studies reported here. Complexes **2**−**4** were characterized by high resolution mass spectrometry and ^{1}H NMR (COSY, NOESY, TOCSY, and HSQC) allowing full assignment of all resonances. X-ray crystal structures of **2** and **3** were also obtained (Supporting Information, Figures S2 and S3).

dx.doi.org/10.1021/ic501032t | *Inorg. Chem.* 2014, 53, 11882−11889

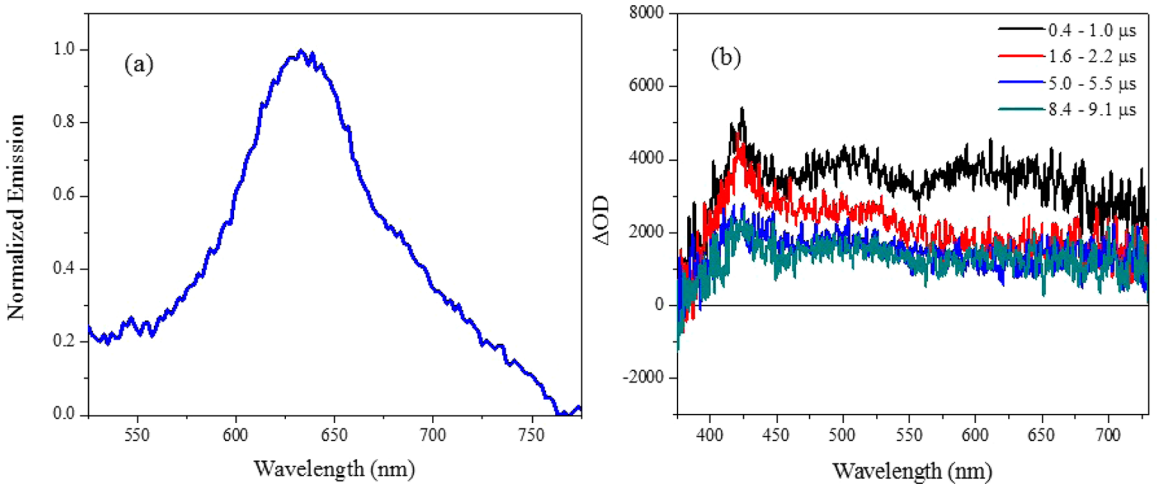

Figure 1. (a) Steady-state emission spectrum (λ_{ex} = 400 nm) and (b) transient absorption spectra (λ_{ex} = 355 nm) of 2 wt % of **1** in a PMMA film (thickness ≈ 300 μm) at time delays shown.

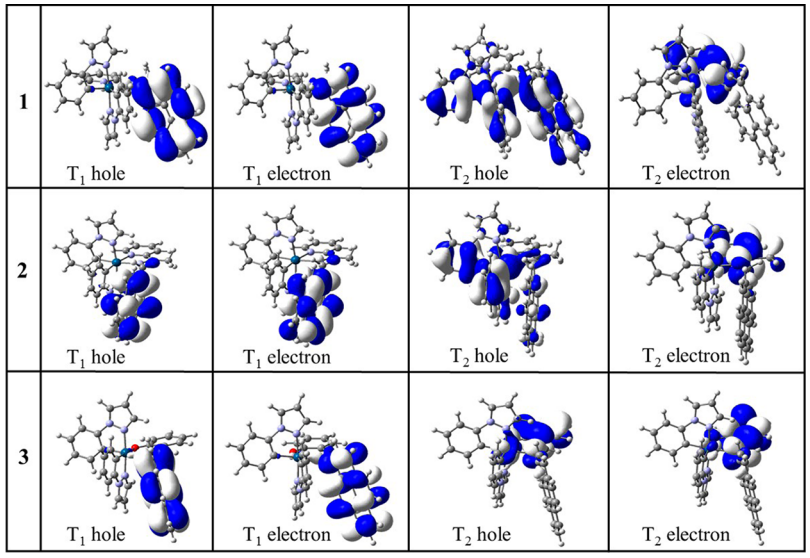

Figure 2. Natural transition orbitals representing the lowest-lying triplet states T_1 and T_2 for complexes **1**−**3** computed from TD-DFT at the SDD09/D95(d)/M06/DCM level of theory.

The absorption spectra of **1**−**3** show phenylpyrazole π−π^* transitions below 300 nm[34] as well as pyrene π−π^* transitions from 270 to 375 nm.[35] The low-energy absorptions above 400 nm are assigned to spin forbidden ^{3}MLCT transitions (Supporting Information, Figure S4a).[36] Similar phenylpyrazole π−π^* transitions below 300 nm as well as spin-forbidden ^{3}MLCT transitions are observed in model complexes **4** and **5** (Supporting Information, Figure S4b). It is important to note that the pyrene π−π^* transitions are well-resolved from the ^{3}MLCT transitions in **1**−**3** and retain strong vibronic coupling, characteristic of pyrene, suggesting weak electronic coupling between the two components. The absorption spectra of 2 wt % of **1**−**3** dispersed in a PMMA film (Supporting Information, Figure S5) are qualitatively similar to the spectra obtained in solution consistent with isolated molecules present in the films.

Complex **1** is not emissive in solution[37] but shows very weak emission (λ_{max} = 631 nm, Φ_{em} = 0.004) when dispersed in a PMMA film (Figure 1). This emission profile is independent of excitation wavelength when λ_{ex} = 325−475 nm. Below the glass transition temperature of PMMA (T_g = 114 °C), molecules dispersed in this polymer are assumed to be isolated from each other in the solid state,[38] with properties similar to those observed in dilute solution.[39] The emission decay from **1** in PMMA fits well to a biexponential function consisting of two components with lifetimes of 329 ns and 2.4 μs, respectively (Supporting Information, Figure S7). The transient absorption spectrum of **1** in a PMMA film shows features attributed to ^{3}pyrene at 420 and 500 nm,[6a,40] as well as broad absorption features attributed to a ^{3}MLCT state at 500 and 625 nm.[41] The decay of the transient species is also biexponential with lifetimes of 378 ns and 2.9 μs, similar to the emission lifetimes observed (Supporting Information, Figure S8). In addition, the time-resolved emission spectrum of **1** in PMMA shows two different bands that decay at different rates (Supporting Information, Figure S9). This "dual emission" can be assigned to decay of ^{3}MLCT and ^{3}pyrene states, respectively. Dual emission from both a ^{3}MLCT state and ^{3}LC state on pyrene has previously been observed at room temperature in solution in Ru(II)-appended pyrenylethynylene dyads,[10] as well as in Ru(II) diimine dyads,[42] and can occur when there is weak

dx.doi.org/10.1021/ic501032t | Inorg. Chem. 2014, 53, 11882−11889

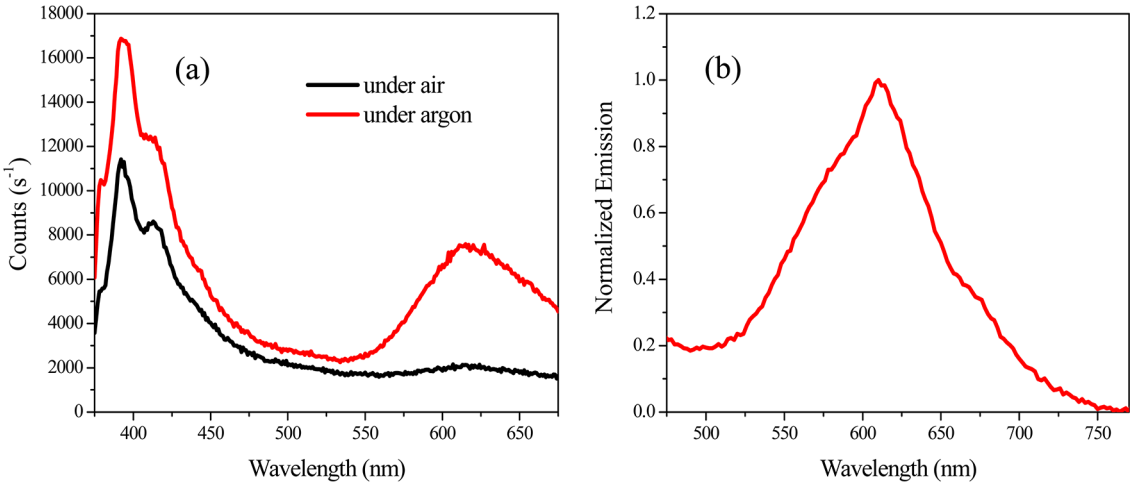

Figure 3. (a) Steady-state emission spectra of **2** in dichloromethane in air (black line) and under argon (red line) (λ_{ex} = 350 nm) and (b) steady-state emission spectrum (λ_{ex} = 400 nm) of 2 wt % of **2** in a PMMA film (thickness ≈ 300 μm).

electronic coupling between the states. This type of dual emission has not been reported for Ir(III)-pyrene complexes, although there are a few examples of nonpyrene containing Ir(III) complexes that display this phenomenon.[43] Dual emission has also been previously observed in rigid matrices at 77 K in Ru(II) complexes bearing pyrenyl ligands.[40,44] To observe dual emission, two excited states must be present that (i) can be populated by the same absorption event, (ii) are separated by an energy barrier that prevents the interconversion of populations, and (iii) exhibit sufficiently different luminescence properties (energy and excited-state lifetimes) to distinguish one state from the other in practical experiments.[45] There are a few possible explanations for the dual emission observed in **1**: (i) similar to glassy matrices, polymer films can give rise to an inhomogeneous environment where some environments may favor ^{3}MLCT emission, while others favor ^{3}LC emission[46] or (ii) the ^{3}MLCT and ^{3}LC states lie close in energy and due to weak electronic coupling between these states, facilitated by the molecular rigidity of the complex inside the polymer film, interconversion of ^{3}MLCT and ^{3}LC populations does not occur, and therefore full relaxation to the lowest lying state does not occur.

DFT calculations were carried out on complex **1** to obtain the natural transition orbitals which give insight into the origin of the lowest-lying triplet states. Natural transition orbitals[30] can be used to visualize the origin and destination orbitals involved in monoelectronic excitations. Natural transition orbital analysis generates a new set of orbitals that allows description of the electronic transition in terms of two of these new orbitals, one describing the hole resulting from the expulsion of one electron and the other describing the orbital housing the expelled electron. In complex **1**, the lowest-lying triplet state (T_1, Figure 2) is localized on the pyrene moiety, consistent with T_1 being exclusively ^{3}pyrene in nature. T_2 is a mixed charge-transfer state from a mixed metal + a ligand orbital to a ligand orbital (Figure 2). It is not uncommon for the emissive state (typically T_1) in bis-cyclometalated Ir(III) complexes to be attributed to a combination of decay from ^{3}MLCT and ^{3}LLCT states[47] or alternatively to a ^{3}MLLCT state.[48] It is rarer, however, to observe a T_1 that is purely ligand-localized (^{3}LC).[47] These calculations support what is observed experimentally as well as the assignment of the two emission bands observed as a $\pi-\pi^*$ state on pyrene (T_1) and a state with significant MLCT character (T_2).

Lengthening the linker between the pyrene and metal is expected to affect the ^{3}MLCT and ^{3}pyrene state energies as well as the degree of electronic coupling between the two states. We chose to replace the pyrene directly bonded to the coordinated nitrogen with one linked via a nonconjugated methylene spacer (complex **2**), as previous studies have shown that ^{3}MLCT emission is quenched in Ir(III) complexes with pyrene directly bound to the ancillary ligand.[7,49]

In contrast to **1**, complex **2** shows broad emission in solution (Figure 3a) at 615 nm with a monoexponential lifetime of 2.7 μs consistent with decay of a ^{3}MLCT state (Supporting Information, Figure S10). This is much longer than the emission lifetime observed for complex **5** with an *N*-isopropyl substituent in place of the *N*-methylenepyrenyl substituent, which has a lifetime of 145 ns in solution.[18] The transient absorption spectrum of **2** in solution shows features attributed to the ^{3}pyrene state[6a,40] at 420 and 500 nm (Supporting Information, Figure S11a). This excited-state absorption decays with a monoexponential lifetime of 3.0 μs (Supporting Information, Figure S12), which is similar to the observed lifetime of the ^{3}MLCT emission. This behavior is typical of reversible energy transfer between ^{3}MLCT and ^{3}pyrene states, giving rise to an extended ^{3}MLCT emission lifetime.[6] Note that complex **2** also shows ^{1}pyrene emission in solution at 400 nm, which decays with a short lifetime (<10 ns) (Supporting Information, Figure S13). It is likely that this emission lifetime represents the time it takes for Förster energy transfer to occur from the ^{1}pyrene state to the ^{1}MLCT state, effectively quenching the ^{1}pyrene emission.

In a PMMA film, complex **2** shows emission at 610 nm with weak shoulders (Figure 3b). Emission lifetimes of 2.0 and 28.1 μs are obtained from a biexponential fit of the emission decay data (Supporting Information, Figure S14). The emission profile is independent of the excitation wavelength when λ_{ex} is between 315 and 475 nm. Similar to **1**, dual emission is observed in the time-resolved emission spectrum (Supporting Information, Figure S15) and can be attributed to radiative decay of ^{3}MLCT (2.0 μs) and ^{3}pyrene (28.1 μs) states. The biexponential decay and the presence of two bands in the time-resolved emission spectrum of **2** in PMMA suggests that the reversible energy transfer between the two states observed in

dx.doi.org/10.1021/ic501032t | *Inorg. Chem.* 2014, 53, 11882−11889

Table 1. Photophysical Properties of Iridium Complexes 1−5 in Dichloromethane and PMMA[a]

	λ_{em} (DCM, nm)	τ_{em} (DCM, μs)	Φ_{em} (DCM)	λ_{em} (PMMA, nm)	τ_{em1} (PMMA, μs)	τ_{em2} (PMMA, μs)	τ_{es} (DCM, μs)	τ_{es1} (PMMA, μs)	τ_{es2} (PMMA, μs)	Φ_{em} (PMMA)
1				631	0.329	2.4		0.378	2.9	0.004
2	615	2.7	0.014[b]	610	2.0	28.1	3.0		35.2	0.028
3				615	18.0	104			101	0.150
4				583	0.046	0.198				0.032
5	590	0.145	0.060	572	0.460	0.877				0.047

[a]Subscript "em" is emission and "τ_{es}" is the lifetime of the excited state. Solution data obtained under argon, and PMMA data obtained in air. [b]Quantum yield of emission at 615 nm (does not include ^{1}pyrene emission).

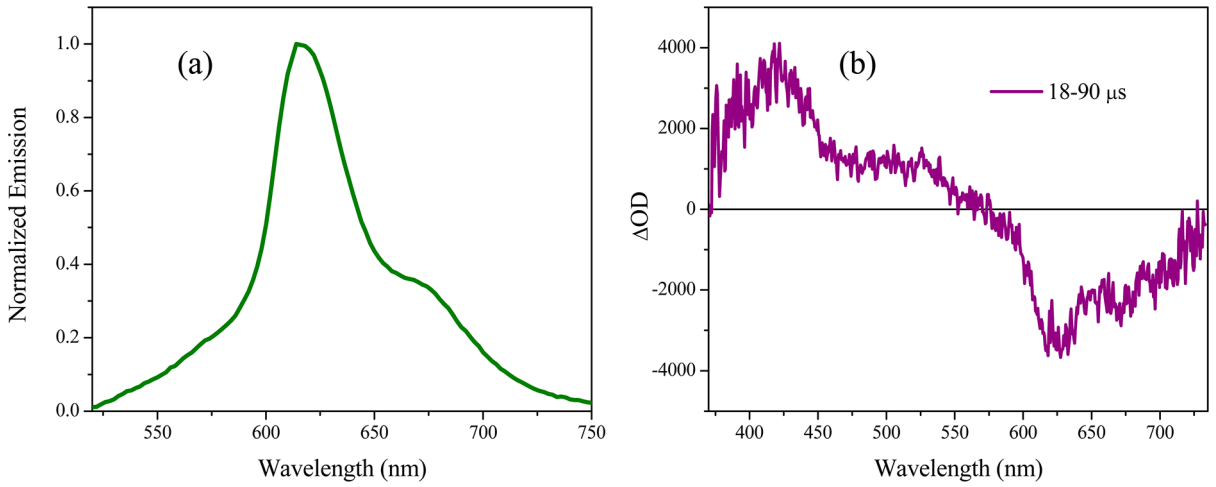

Figure 4. (a) Steady state emission spectrum (λ_{ex} = 400 nm) and (b) transient absorption spectrum (λ_{ex} = 355 nm) of 2 wt % of **3** in a PMMA film (thickness ≈ 200 μm) at a time delay of 18−90 μs.

solution is no longer effective within the PMMA film. Two possible explanations for this are (i) molecular rigidity within the solid polymer matrix prevents back-folding of the pyrene ligand, and therefore only one conformation is present. This leads to a fixed orientation of the two interacting triplet states, which can affect the electronic coupling as well as the transition dipole moments of the two states having an effect on energy transfer rates;[42] (ii) in complexes **2** and **5** the energy of the charge-transfer state increases in the PMMA film relative to in solution (Table 1). If the energy of the ^{3}LC state on pyrene remains relatively unperturbed, this would effectively increase the energy gap between the ^{3}MLCT and ^{3}LC states in PMMA, possibly making thermal population of the ^{3}MLCT state no longer feasible at room temperature. This is similar to the solvent dependent behavior of reversible energy transfer that has been observed in bichromophoric Ru(II) complexes, where the ^{3}MLCT state is only thermally accessible in methanol, but shifts higher in energy in water and acetonitrile and is not populated in these solvents.[50]

The transient absorption spectrum of **2** in PMMA shows features attributed to the ^{3}pyrene state[6a,40] at 420 and 500 nm (Supporting Information, Figure S11b). In contrast to complex **1**, there is no evidence for ^{3}MLCT excited-state absorptions in **2**, and the transient of **2** decays with a monoexponential lifetime of 35.2 μs (Supporting Information, Figure S16). This lifetime is similar to the long-lived emission component further confirming that this emission originates from a ^{3}LC state on pyrene. DFT calculations were used to obtain the natural transition orbitals for complex **2**, and these show that the lowest lying triplet state (T_1, Figure 2) is localized on the pyrene moiety, consistent with T_1 being exclusively ^{3}pyrene in nature. T_2 is a mixed charge-transfer state from a mixed metal + ligand orbital to a ligand localized orbital (Figure 2). These calculations support what is observed experimentally and fit the criteria necessary for the triplet reservoir effect or dual emission to be observed; that is, T_1 is a $\pi-\pi^*$ state on pyrene, while T_2 has significant MLCT character.

Complex **3** is structurally related to **1** with only two bonds separating the metal and pyrene groups, but with a salicylimine-based ancillary ligand. Ir(III) complexes bearing salicylimine ligands are known to be more strongly emissive in the solid state than Ir(III) pyridineimine derivatives.[51] Complex **3** is not emissive in solution at room temperature. This lack of emission is attributed to nonradiative decay caused by distortions of the six-membered O^N chelate ring relative to the equatorial plane of the molecule. We have previously reported a series of iridium complexes containing salicylimine (O^N) ligands, which are not emissive in solution as a result of the presence of this nonradiative decay pathway.[32] DFT calculations show that **3** undergoes similar distortions (Supporting Information, Figure S17), consistent with the lack of emission from **3** at room temperature in solution. The O^N-aryl complexes we reported previously display broad unstructured phosphorescence emission in the solid state and in PMMA arising from a ^{3}MLLCT type state.[32] In contrast, **3** shows structured phosphorescence in the solid state centered at 615 nm, the profile of which remains identical with excitation in the range of λ_{ex} = 315−475 nm. When dispersed in PMMA, **3** shows moderately intense structured phosphorescence (Φ_{em} = 0.150) at 615 nm (Figure 4a) with lifetimes of 18.0 and 104 μs obtained by fitting to a biexponential function (Supporting Information, Figure S18), consistent with dual ^{3}MLCT and ^{3}LC emission. The transient

dx.doi.org/10.1021/ic501032t | Inorg. Chem. 2014, 53, 11882−11889

absorption spectrum of **3** in a PMMA film shows an excited-state absorption typical of ^{3}pyrene[6a,40] at 420 and 500 nm (Figure 4b), which decays monoexponentially with a lifetime of 101 μs (Supporting Information, Figure S19) as well as a negative signal at 615 nm, which corresponds to stimulated emission from the complex. This excited-state lifetime corresponds to the long-lived component of the emission supporting the conclusion that the long-lived emission is from a ^{3}LC state. DFT calculations, used to obtain the natural transition orbitals for complex **3**, show that the lowest-lying triplet (T_1) is localized on pyrene, whereas T_2 is calculated to be a mixed charge-transfer state from a mixed metal + ligand orbital to a ligand orbital involving primarily the salicylimine moiety of the ancillary ligand. In contrast to complexes **1** and **2**, the phenylpyrazole ligands do not contribute to the calculated T_1 or T_2 states in complex **3**. The calculations support the assignment of dual emission with a pyrene (T_1) and MLCT (T_2) component.

Complexes **4** and **5** also show biexponential emission decay curves in PMMA (Supporting Information, Figures S20 and S21, respectively) with both lifetimes being less than 1 μs. In contrast to complexes **1**−**3**, the time-resolved emission spectra of complexes **4** and **5** in PMMA (Supporting Information, Figure S22) show only one broad emission band over time. The origin of the biexponential emission decay observed from complexes **4** and **5** in PMMA is not clear. Without the observation of two distinct bands in the time-resolved emission spectrum this biexponential decay cannot be clearly assigned to two different emitting states. Studies on luminescent metal complexes embedded in polymer matrices have previously shown multiexponential emission decay. These multiexponential decay kinetics have been attributed to different microenvironments within the polymer matrix resulting in different emission lifetimes.[52] While the emission decay curves of complexes **1**−**5** in PMMA fit most closely to a biexponential function, it is possible that contributions from multiple different local environments around the emitter molecules play a role.[53] The behavior of complexes **1**−**3** in PMMA is clearly different than that of **4** and **5** as evidenced from the time-resolved emission spectra and lifetimes of these complexes (Supporting Information, Figure S22). Natural transition orbital analysis performed on model complexes **4** and **5**, show that T_1 is a mixed charge-transfer state from a metal + ligand to ligand orbital (Supporting Information, Figure S23), analogous to T_2 in complexes **1**-**3**, and similar to what is observed most commonly as the T_1 state in bis-cyclometalated Ir(III) complexes.[45,46] This is consistent with the lowest-lying triplet state of **4** and **5** having significant ^{3}MLCT character.

CONCLUSION

In summary, complexes **1**−**3** are the first examples of iridium complexes that show dual emission in solid matrices resulting from ^{3}MLCT and long-lived ^{3}LC states on pyrene. Complex **2** represents a significant addition to the small family of iridium complexes showing extended lifetimes due to excited-state equilibration in solution. Coordination complexes with extended emission and excited-state lifetimes are relevant to photoredox catalysis and upconversion applications. In addition, the kinetic inertness of low-spin d^6 octahedral complexes such as **1**−**3**, large Stokes shifts (>100 nm), and microsecond emission lifetimes makes these complexes potential candidates for time-resolved bioimaging techniques.

ASSOCIATED CONTENT

Supporting Information

Crystal structures, absorption spectra, time-resolved emission spectra, transient absorption spectra, raw lifetime data, DFT calculations, and CIF files. This material is available free of charge via the Internet at http://pubs.acs.org.

AUTHOR INFORMATION

Corresponding Author

*E-mail: mwolf@chem.ubc.ca.

Notes

The authors declare no competing financial interest.

ACKNOWLEDGMENTS

This work was supported by the Natural Sciences and Engineering Research Council of Canada. D.L.D. thanks the Leverhulme Trust for a study abroad fellowship, F.L. thanks Consorzio INSTM for financial support and the Department of Chemistry at UBC for the hospitality during a visiting leave from Italy.

REFERENCES

(1) (a) Finikova, O. S.; Lebedev, A. Y.; Aprelev, A.; Troxler, T.; Gao, F.; Garnacho, C.; Muro, S.; Hochstrasser, R. M.; Vinogradov, S. A. *ChemPhysChem* **2008**, *9*, 1673−1679. (b) Kondrashina, A. V.; Dmitriev, R. I.; Borisov, S. M.; Klimant, I.; O'Brien, I.; Nolan, Y. M.; Zhdanov, A. V.; Papkovsky, D. B. *Adv. Funct. Mater.* **2012**, *22*, 4931−4939. (c) Gu, L.; Hall, D. J.; Qin, Z.; Anglin, E.; Joo, J.; Mooney, D. J.; Howell, S. B.; Sailor, M. J. *Nat. Commun.* **2013**, *4*, 2326−2332.

(2) (a) Goldsmith, J. I.; Hudson, W. R.; Lowry, M. S.; Anderson, T. H.; Bernhard, S. *J. Am. Chem. Soc.* **2005**, *127*, 7502−7510. (b) Zeitler, K. *Angew. Chem., Int. Ed.* **2009**, *48*, 9785−9789. (c) Prier, C. K.; Rankic, D. A.; MacMillan, D. W. C. *Chem. Rev.* **2013**, *113*, 5322−5363.

(3) Singh-Rachford, T. N.; Castellano, F. N. *Coord. Chem. Rev.* **2010**, *254*, 2560−2573.

(4) (a) Liu, S.; Sun, H.; Ma, Y.; Ye, S.; Liu, X.; Zhou, X.; Mou, X.; Wang, L.; Zhao, Q.; Huang, W. *J. Mater. Chem.* **2012**, *22*, 22167−22173. (b) Lloyd, D.; Coogan, M. P.; Pope, S. J. A. *Rev. Fluoresc.* **2010**, 15−44.

(5) Turro, N. J. *Modern Molecular Photochemistry;* University Science Books: Sausalito, CA, 1991.

(6) (a) Ford, W. E.; Rodgers, M. A. J. *J. Phys. Chem.* **1992**, *96*, 2917−2920. (b) Lavie-Cambot, A.; Lincheneau, C.; Cantuel, M.; Leydet, Y.; McClenaghan, N. D. *Chem. Soc. Rev.* **2010**, *39*, 506−515. (c) Tyson, D. S.; Castellano, F. N. *J. Phys. Chem. A* **1999**, *103*, 10955−10960.

(7) Denisov, S. A.; Cudré, Y.; Verwilst, P.; Jonusauskas, G.; Marín-Suárez, M.; Fernández-Sánchez, J. F.; Baranoff, E.; McClenaghan, N. D. *Inorg. Chem.* **2014**, *53*, 2677−2682.

(8) Omary, M. A.; Kassab, R. M.; Haneline, M. R.; Elbjeirami, O.; Gabbai, F. B. *Inorg. Chem.* **2003**, *42*, 2176−2178.

(9) Hua, F.; Kinayyigit, S.; Rachford, A.; Shikhova, E. A.; Goeb, S.; Cable, J. R.; Adams, C. J.; Kirschbaum, K.; Pinkerton, A. A.; Castellano, F. N. *Inorg. Chem.* **2007**, *46*, 8771−8783.

(10) Lincoln, R.; Kohler, L.; Monro, S.; Yin, H.; Stephenson, M.; Zong, R.; Chouai, A.; Dorsey, C.; Hennigar, R.; Thummel, R. P.; McFarland, S. A. *J. Am. Chem. Soc.* **2013**, *135*, 17161−17175.

(11) Avilov, I.; Minoofar, P.; Cornil, J.; De Cola, L. *J. Am. Chem. Soc.* **2007**, *129*, 8247−8258.

(12) Hu, J.; Yip, J. H. K.; Ma, D.-L.; Wong, K.-Y.; Chung, W.-H. *Organometallics* **2009**, *28*, 51−59.

(13) Davies, D. L.; Lowe, M. P.; Ryder, K. S.; Singh, K.; Singh, S. *Dalton Trans.* **2011**, *40*, 1028−1030.

(14) Bavin, P. M. G.; Dewar, M. J. S. *J. Chem. Soc.* **1956**, 164−169.

(15) Matkovich, K. M. M.Sc. Thesis, University of British Columbia: Vancouver, BC, 2009.

(16) Kim, H. J.; Bhuniya, S.; Mahajan, R. K.; Puri, R.; Liu, H.; Ko, K. C.; Lee, J. Y.; Kim, J. S. *Chem. Commun.* **2009**, 7128−7130.
(17) Howarth, A. J.; Davies, D. L.; Lelj, F.; Wolf, M. O.; Patrick, B. O. *Dalton Trans.* **2012**, *41*, 10150−10152.
(18) Davies, D. L.; Lelj, F.; Lowe, M. P.; Ryder, K. S.; Singh, K.; Singh, S. *Dalton Trans.* **2014**, *43*, 4026−4039.
(19) *SAINT, Version 7.68A;* Bruker AXS, Inc.: Madison, WI, 1997−2010.
(20) *TWINABS;* Sheldrick, G. M.; *Acta Crystallogr.* **2008**, *A64*, 112−122.
(21) *SADABS;* Bruker AXS, Inc.: Madison, WI, 1997−2012.
(22) Becke, A. D. *J. Chem. Phys.* **1997**, *107*, 8554−8560.
(23) Adamo, C.; Barone, V. *J. Comput. Chem.* **1998**, *19*, 418−429.
(24) Adamo, C.; Barone, V. *J. Chem. Phys.* **1999**, *110*, 6158−6169.
(25) Yanai, T.; Tew, D.; Handy, N. *Chem. Phys. Lett.* **2004**, *393*, 51−57.
(26) Zhao, Y.; Truhlar, D. G. *Theor. Chem. Acc.* **2008**, *120*, 215−241.
(27) Dunning Jr., T. H.; Hay, P. J. In *Modern Theoretical Chemistry;* Plenum: New York, 1976.
(28) Figgen, D.; Peterson, K. A.; Dolg, M.; Stoll, H. *J. Chem. Phys.* **2009**, *130*, 164108.
(29) Casida, M. E. In *Recent Advances in Density Functional Methods;* Chong, D. P., Ed.; World Scientific: Singapore, 1995.
(30) Martin, R. L. *J. Chem. Phys.* **2003**, *118*, 4775−4777.
(31) Frisch, M. J.; Trucks, G. W.; Schlegel, H. B.; Scuseria, G. E.; Robb, M. A.; Cheeseman, J. R.; Scalmani, G.; Barone, V.; Mennucci, B.; Petersson, G. A.; Nakatsuji, H.; Caricato, M.; Li, X.; Hratchian, H. P.; Izmaylov, A. F.; Bloino, J.; Zheng, G.; Sonnenberg, J. L.; Hada, M.; Ehara, M.; Toyota, K.; Fukuda, R.; Hasegawa, J.; Ishida, M.; Nakajima, T.; Honda, Y.; Kitao, O.; Nakai, H.; Vreven, T.; Montgomery, J. A., Jr.; Peralta, J. E.; Ogliaro, F.; Bearpark, M.; Heyd, J. J.; Brothers, E.; Kudin, K. N.; Staroverov, V. N.; Kobayashi, R.; Normand, J.; Raghavachari, K.; Rendell, A.; Burant, J. C.; Iyengar, S. S.; Tomasi, J.; Cossi, M.; Rega, N.; Millam, N. J.; Klene, M.; Knox, J. E.; Cross, J. B.; Bakken, V.; Adamo, C.; Jaramillo, J.; Gomperts, R.; Stratmann, R. E.; Yazyev, O.; Austin, A. J.; Cammi, R.; Pomelli, R.; Ochterski, J. W.; Martin, R. L.; Morokuma, K.; Zakrzewski, V. G.; Voth, G. A.; Salvador, P.; Dannenberg, J. J.; Dapprich, S.; Daniels, A. D.; Farkas, Ö.; Foresman, J. B.; Ortiz, J. V.; Cioslowski, J.; Fox, D. J. *Gaussian 09, Revision D.1;* Gaussian, Inc.: Wallingford, CT, 2009.
(32) Howarth, A. J.; Patia, R.; Davies, D. L.; Lelj, F.; Wolf, M. O.; Singh, K. *Eur. J. Inorg. Chem.* **2014**, DOI: 10.1002/ejic.201402495.
(33) Konno, H.; Sasaki, Y. *Chem. Lett.* **2003**, *32*, 252−253.
(34) Wu, W.; Guo, H.; Wu, W.; Ji, S.; Zhao, J. *Inorg. Chem.* **2011**, *50*, 11446−11460.
(35) Dillon, R. J.; Bardeen, C. J. *J. Phys. Chem. A* **2012**, *116*, 5145−5150.
(36) Calogero, G.; Giuffrida, G.; Serroni, S.; Ricevuto, V.; Campagna, S. *Inorg. Chem.* **1995**, *34*, 541−545.
(37) The lack of emission in solution and the presence of very weak emission in the solid state at room temperature are attributed to a distortion of the imine N in this complex, which gives rise to a nonradiative decay pathway. See ref 18 for more details.
(38) Complexes **1**−**3** have the same emission profile when 1, 2, 5, or 10 wt % of each complex is dispersed in PMMA (Supporting Information, Figure S6). While this does not rule out the possibility of aggregation at these concentrations, it suggests that aggregation effects are not significant.
(39) (a) Fukaminato, T.; Umemoto, T.; Iwata, Y.; Yokojima, S.; Yoneyama, M.; Nakamura, S.; Irie, M. *J. Am. Chem. Soc.* **2007**, *129*, 5932−5938. (b) He, L.; Duan, L.; Qiao, J.; Wang, R.; Wei, P.; Wang, L.; Qiu, Y. *Adv. Funct. Mater.* **2008**, *18*, 2123−2131. (c) Au, K.-M.; Wong, K. M.-C.; Tsang, D. P.-K.; Chan, M.-Y.; Zhu, N.; Yam, V. W.-W. *J. Am. Chem. Soc.* **2010**, *132*, 14273−14278.
(40) Wilson, G. J.; Sasse, W. H. F.; Mau, A. W.-H. *Chem. Phys. Lett.* **1996**, *250*, 583−588.
(41) Li, Y.; Dandu, N.; Liu, R.; Hu, L.; Kilina, S.; Sun, W. *ACS. Appl. Mater. Interfaces* **2013**, *5*, 6556−6570.
(42) Leroy-Lhez, S.; Belin, C.; D'Aleo, A.; Williams, R. M.; De Cola, L.; Fages, F. *Supramol. Chem.* **2003**, *15*, 627−637.
(43) (a) Ladouceur, S.; Donato, L.; Romain, M.; Mudraboyina, B. P.; Johansen, M. B.; Wisner, J. A.; Zysman-Colman, E. *Dalton Trans.* **2013**, *42*, 8838−8847. (b) Yeh, Y.-S.; Cheng, Y.-M.; Chou, P.-T.; Lee, G.-H.; Yang, C.-H.; Chi, Y.; Shu, C.-F.; Wang, C.-H. *ChemPhysChem* **2006**, *7*, 2294−2297. (c) Lo, K. K.-W.; Chung, C.-K.; Zhu, N. *Chem.−Eur. J.* **2006**, *12*, 1500−1512. (d) Lo, K. K.-W.; Zhang, K. Y.; Leung, S.-K.; Tang, M.-C. *Angew. Chem., Int. Ed.* **2008**, *47*, 2213−2216.
(44) Simon, J. A.; Curry, S. L.; Schmehl, R. H.; Schatz, T. R.; Piotrowiak, P.; Jin, X.; Thummel, R. P. *J. Am. Chem. Soc.* **1997**, *119*, 11012−11022.
(45) Glazer, E. C.; Magde, D.; Tor, Y. *J. Am. Chem. Soc.* **2007**, *129*, 8544−8551.
(46) Colombo, M. G.; Hauser, A.; Güdel, H. U. *Top. Curr. Chem.* **1994**, *171*, 143−171.
(47) (a) Colombo, M. G.; Guedel, H. U. *Inorg. Chem.* **1993**, *32*, 3081−3087. (b) Colombo, M. G.; Hauser, A.; Guedel, H. U. *Inorg. Chem.* **1993**, *32*, 3088−3092. (c) Lowry, M. S.; Hudson, W. R.; Pascal, R. A.; Bernhard, S. *J. Am. Chem. Soc.* **2004**, *126*, 14129−14135.
(48) Tamayo, A. B.; Garon, S.; Sajoto, T.; Djurovich, P. I.; Tsyba, I. M.; Bau, R.; Thompson, M. E. *Inorg. Chem.* **2005**, *44*, 8723−8732.
(49) Constable, E. C.; Neuburger, M.; Rösel, P.; Schneider, G. E.; Zampese, J. A.; Housecroft, C. E.; Monti, F.; Armaroli, N.; Costa, R. D.; Ortí, E. *Inorg. Chem.* **2013**, *52*, 885−897.
(50) Indelli, M. T.; Ghirotti, M.; Prodi, A.; Chiorboli, C.; Scandola, F.; McClenaghan, N. D.; Puntoriero, F.; Campagna, S. *Inorg. Chem.* **2003**, *42*, 5489−5497.
(51) (a) You, Y.; Huh, H. S.; Kim, K. S.; Lee, S. W.; Kim, D.; Park, S. Y. *Chem. Commun.* **2008**, 3998−4000. (b) Huang, K.; Wu, H.; Sei, M.; Li, F.; Yi, T.; Huang, C. *Chem. Commun.* **2009**, 1243−1245. (c) Zhao, Q.; Li, L.; Li, F.; Yu, M.; Liu, Z.; Yi, T.; Huang, C. *Chem. Commun.* **2008**, 685−687.
(52) Moore, S. A.; Frazier, S. M.; Sibbald, M. S.; DeGraff, B. A.; Demas, J. N. *Langmuir* **2011**, *27*, 9567−9575.
(53) Bauer, R.; Finkenzeller, W. J.; Bogner, U.; Thompson, M. E.; Yersin, H. *Org. Electron.* **2008**, *9*, 641−648.